J19.1 NUMERICAL SIMULATIONS OF AIRFLOWS AND TRANSPORT AND DIFFUSION FROM WIND TUNNEL TO TERRAIN SCALES

Tetsuji Yamada
Yamada Science & Art Corporation, Santa Fe, New Mexico

1. INTRODUCTION

We added CFD (Computational Fluid Dynamics) capabilities to a three-dimensional atmospheric model HOTMAC. The new model is referred to as A2Cflow where "A2C" stands for "Atmosphere to CFD." A single model approach has an attractive feature such that model physics are identical for the CFD and atmospheric components. For example, A2Cflow can simulate airflows from building to terrain scales in a seamless manner by nesting computational domains.

Yamada (2008) presented five simulations to demonstrate the A2C modeling capabilities from wind tunnel to atmospheric simulations. Simulations were conducted to illustrate the thermal effects of building walls on the air flows around two (2) buildings.

When building walls were heated and cooled by the sun, air flows around two buildings became quite different from those without wall heating. Recirculation and reattachment around buildings no longer existed. In general upward motions were simulated along warm walls and downward motions were simulated along cold walls.

Airflows exterior and interior of buildings were also investigated. Building interior flows were influenced by the locations of opening (windows and doors) and exterior flows. Exterior flows, on the other hand, were functions of local circulations resulted from topographic variations.

We simulated diurnal variations of air flows around a cluster of buildings, which were bound by the ocean and hills. Large cities are often located in a coastal area or in complex terrain. Prediction of transport and diffusion of air pollutants and toxic materials is of considerable interest to the safety of the people living in urban areas.

There were significant interactions between air flows generated by topographic variations and a cluster of buildings. Sea breeze fronts were retarded by buildings. Winds were calm in the courtyards. Winds diverged in the upstream side and converged in the downstream side of the building cluster.

In this study, verification studies were conducted by comparing the modeled A2C results with wind tunnel data. Horizontal and vertical grid spacing were decreased to the order of "cm" in order to resolve rectangular obstacles placed in a wind tunnel. Reattachment distance behind an obstacle was compared with wind tunnel data and other model results.

Affiliated with the A2Cflow is a three-dimensional transport and diffusion code "A2Ct&d" where "t&d" stands for transport and diffusion. A2Ct&d is based on a Lagrangian random walk theory (Yamada and Bunker, 1988). A2Cflow provides three-dimensional mean and turbulence distributions to A2Ct&d.

The Lagrangian model requires an integral time scale which influences the correlation between the random velocities generated in the model. The integral time scale was obtained as the ratio between the modeled length scale and velocity scale. The velocity scale was the square root of the turbulence kinetic energy (TKE).

2. MODELS

The governing equations for mean wind, temperature, mixing ratio of water vapor, and turbulence were similar to those used by Yamada and Bunker (1988). Turbulence equations were based on the Level 2.5 Mellor-Yamada second-moment turbulence-closure model (Mellor and Yamada, 1974, 1982).

Five primitive equations were solved for ensemble averaged variables: three wind components, potential temperature, and mixing ratio of water vapor. In addition, two primitive equations were

solved for turbulence: one for TKE and the other for a turbulence length scale (Yamada, 1983).

The hydrostatic equilibrium is a good approximation in the atmosphere. On the other hand, air flows around buildings are not in the hydrostatic equilibrium. Pressure variations are generated by changes in wind speeds, and the resulted pressure gradients subsequently affect wind distributions.

We adopted the HSMAC (Highly Simplified Marker and Cell) method (Hirt and Cox, 1972) for non-hydrostatic pressure computation because the method is simple yet efficient. The method is equivalent to solving a Poisson equation, which is commonly used in non-hydrostatic atmospheric models.

Boundary conditions for the ensemble and turbulence variables were discussed in detail in Yamada and Bunker (1988). The temperature in the soil layer was obtained by numerically integrating a heat conduction equation. Appropriate boundary conditions for the soil temperature equation were the heat energy balance at the ground and specification of the soil temperature at a certain distance below the surface, where temperature was constant during the integration period. The surface heat energy balance was composed of solar radiation, long-wave radiation, sensible heat, latent heat, and soil heat fluxes.

Lateral boundary values for all predicted variables were obtained by integrating the corresponding governing equations, except that variations in the horizontal directions were all neglected. The upper level boundary values were specified and these values were incorporated into the governing equations through four-dimensional data assimilation or a “nudging” method (Kao and Yamada, 1988).

Temperatures of building walls and roofs were computed by solving a one-dimensional heat conduction equation in the direction perpendicular to the walls and roofs. One boundary condition was a heat energy balance equation at the outer sides of walls and roofs. Another boundary condition was the room temperatures specified at the inner sides of the walls.

Mellor-Yamada turbulence closure equations were in three-dimensional where derivatives in x, y, and z (vertical) directions were included. HOTMAC adopted the boundary layer approximation where derivatives in x and y directions were neglected in comparison with those in z direction. The boundary layer approximation was valid for mesoscale simulations where horizontal grid spacing was significantly larger than the vertical grid spacing. Consequently, horizontal derivatives became negligible in comparison with those in the vertical direction.

The production terms in the TKE and length scale equations should include horizontal derivatives for CFD simulations. The production terms in the horizontal and vertical directions are in the same order of magnitudes since the horizontal and vertical grid spacing are comparative.

Turbulence fluxes in the standard k-e models were modeled by the following down-gradient relationships.

$$-\overline{u_i u_j} = \nu_t \left(\frac{\partial U_i}{\partial x_j} + \frac{\partial U_j}{\partial x_i}\right) \tag{1}$$

This method is known to overestimate TKE at the impinging area of the building walls. Various approaches were proposed to mitigate the issue (e.g.,Tominaga et al, 2008).

In the present study, the following relationships were used.

$$\overline{w^2} - \overline{u^2} \approx \overline{w^2} - \overline{v^2} \tag{2}$$

$$\begin{aligned} \overline{u^2} &= (1-2\gamma_1)q^2 \\ \overline{v^2} &= \overline{w^2} = \gamma_1 q^2 \end{aligned} \tag{3}$$

$$\gamma_1 = 0.222 \tag{4}$$

Relationships (3) and (4) were obtained by the Level 2 model of Mellor and Yamada (1982).

The TKE equation includes the following production terms which are related to impingement:

$$\begin{aligned} P_k &= -\overline{uu}\frac{\partial U}{\partial x} - \overline{vv}\frac{\partial V}{\partial y} - \overline{ww}\frac{\partial W}{\partial z} - \cdots\cdots \\ &= (\overline{w^2} - \overline{u^2})\frac{\partial U}{\partial x} + (\overline{w^2} - \overline{v^2})\frac{\partial V}{\partial y} \cdots\cdots \end{aligned} \tag{5}$$

where the mass conservation equation was used to eliminate $\partial W/\partial z$ in the first line. The production terms included many other terms which were modeled by the down-gradient relationship (1) and included in A2C.

Here only the terms related to impingement were discussed. Murakami (2000) identified that the cause of the TKE overestimation: the impingement terms became very large if they were modeled by using the down-gradient relationship. Murakami also discussed various proposals to mitigate the issue.

In this study, the down- gradient relationship was not used to model the impingement terms. Instead, we used the Mellor-Yamada Level 2 relationships as in (3). Substituting an assumption (2) into (5), the impingement terms became

$$\begin{aligned} P_k &= (\overline{w^2} - \overline{u^2})(\frac{\partial U}{\partial x} + \frac{\partial V}{\partial y}) \ldots\ldots \\ &= -(3\gamma_1 - 1)q^2 \frac{\partial W}{\partial z} \ldots\ldots \\ &= 0.334 q^2 \frac{\partial W}{\partial z} \ldots\ldots \end{aligned} \quad (6)$$

where relationships (3) and (4) and the mass conservation equation were used. Note that the coefficient of the impingement terms in the first line of (6) is the difference between the two turbulence components. If the flow were in isotropic, the coefficient became zero and so did the impingement terms.

The final form of (6) became independent of horizontal derivatives which assured symmetry of the model results for various wind directions. This feature was discussed in the next section.

3. SIMULATIONS

1. Wind Tunnel Model Simulation

Wind tunnel experiments were conducted under well controlled conditions (in comparison with field campaigns) and extensive measurements were available for verification of model results. We selected three cases from the wind tunnel experiments reported in Tominaga et al. (2008).

A first simulation was conducted in a computational domain of 100 cm x 50 cm x 100 cm (vertical) with horizontal grid spacing of 1 cm. The vertical grid spacing was 2 cm for the first 30 cm from the ground and increased gradually to the top of computational domain.

A model building of 10 cm (W) x 10 cm (D) x 20 cm (H) was placed along the centerline of the computational domain (2:1:1 block). Inflow boundary values of winds and TKE were specified by the measurements.

Steady state solutions were obtained when boundary conditions were kept constant and integration continued until flow fields became visibly unchanged.

Figure 1 shows wind direction (arrows) and wind speed (color) distributions in a vertical cross section along the centerline of the computational domain.

There was upward motion at the leading edge of the building, which resulted in separation and recirculation of air flows along the roof. Separation of air flows also occurred at the rear side of the building. The modeled characteristics of recirculation and reattachment were in good qualitative agreement with wind tunnel data.

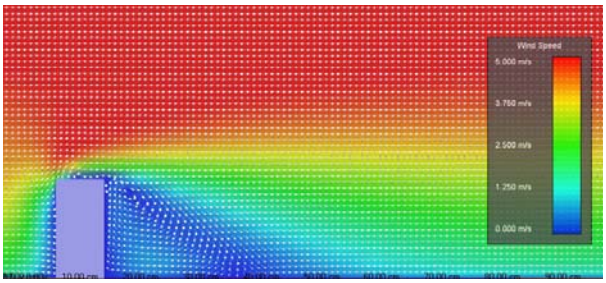

Fig. 1: The modeled wind distributions in a vertical cross section along the centerline of the computational domain

A second simulation was conducted in a computational domain of 100 cm cube where a block of 20 cm (W) x 5 cm (D) x 20 cm (H) (4:4:1 block) was placed along the centerline of the computational domain. Horizontal and vertical grid spacing were the same as for the first case. Inflow boundary conditions were specified from the measurements.

Figure 2 shows wind direction (arrows) and wind speed (color) distributions in a vertical cross section along the centerline of the computational domain. The reattachment distance was significantly larger than the counterpart of the first case because the block was twice wider.

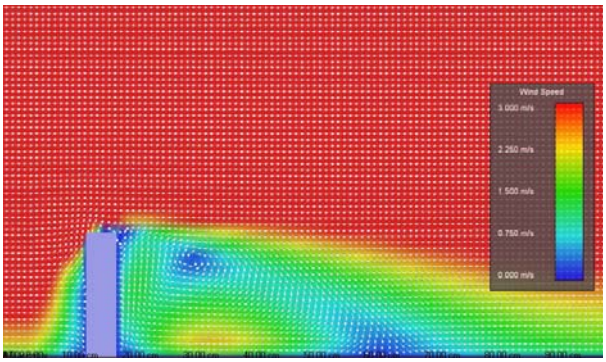

Fig. 2: The modeled wind distributions in a vertical cross section along the centerline of the computational domain

Table 1 shows comparison of the reattachment distance from the back side of a block among various models and wind tunnel measurements.

	2:1:1 block (cm)	4:4:1 block (cm)
wind tunnel	14	38
LES	10-21	38
k-e	20-33	46-68
k-l (A2C)	27	40

Table 1: Comparison of reattachment distance between wind tunnel measurements and various models. The model results except A2C were from Architectural Institute of Japan (2007)

A third simulation was conducted in a computational domain of 200 cm x 200 cm x 100 cm (vertical) where nine blocks of 10 cm cube were placed except the center one whose height was 20 cm (Fig. 3).

Fig.3: Computational domain of 200 cm x 200 cm x 100 cm (vertical). Horizontal grid spacing was 2 cm. Vertical grid spacing was 2 cm for the first 50 cm and increased with height.

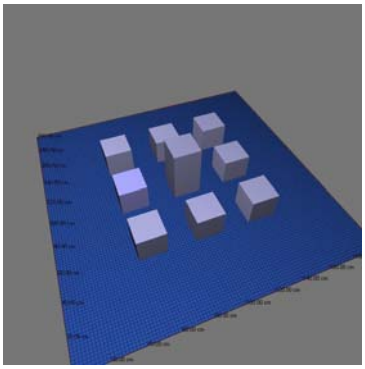

Inflow wind directions were varied by 90 degrees to test symmetry of the model results. Figure 4 and 5 shows the modeled wind speed and TKE distributions at 2 cm above the floor for various wind directions.

Both wind and TKE distributions were approximately symmetric. Slightly better results were obtained for TKE than wind speed. The areas of asymmetry are mainly in the area where wind speeds were very small (blue color).

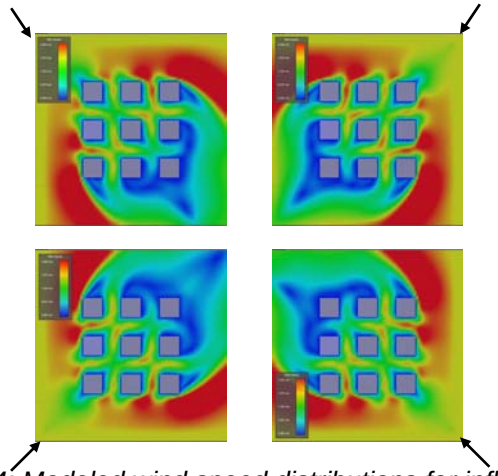

Fig. 4: Modeled wind speed distributions for inflow wind directions of 45, 135, 225, and 315 degrees (clock wise from upper-left image)

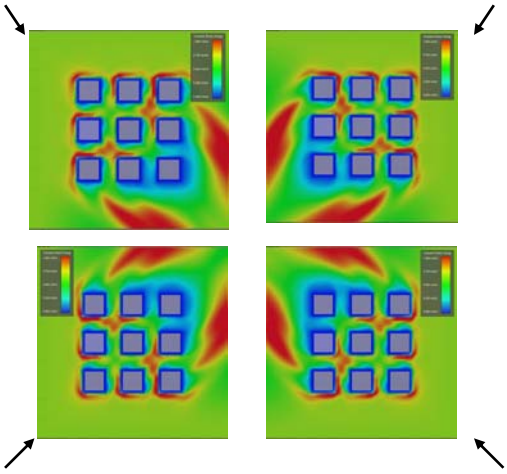

Fig. 5: Modeled TKE distributions for inflow wind directions of 45, 135, 225, and 315 degrees (clock wise from upper-left image)

2. Lagrangian Integral Time

A2Ct&d is based on Lagrangian random particle algorithm.

$$x_i(t+\Delta t) = x_i(t) + U_{pi}\Delta t,$$

$$U_{pi} = U_i + u_i,$$

$$u_i(t+\Delta t) = a u_i(t) + b\sigma_{ui}\xi + \delta_{i3}(1-a)t_{Lx_i}\frac{\partial}{\partial x_i}(\sigma_{u_i}^2),$$

$$a = \exp(-\Delta t / t_{Lx_i}), \quad b = (1-a^2)^{1/2}$$

t_{Lx_i} is the Lagrangian integral time. A2C used constant values for the Lagrangian integral time as listed in Table 2.

mesoscale (s)	building (s)	wind tunnel (s)
10000	10-20	0.01-0.1
20	10-20	0.01-0.1

Table 2: Typical values of Lagrangian time scale used in A2C for mesoscale, building, and wind tunnel simulations, resplectively

Figure 6 shows the modeled TKE, length scale, and time scale for a 2:1:1 block in the vertical cross section along the centerline of the computational domain.

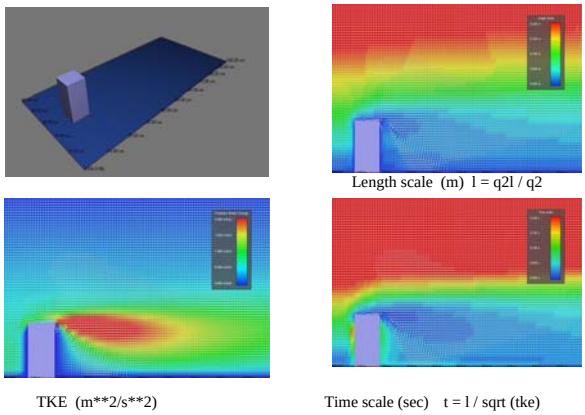

Fig. 6: The modeled TKE, length scale, and time scale for a 2:1:1 block in the vertical cross section along the centerline of the computational domain

The modeled time scale in Fig. 6 shows distributions inversely proportional to TKE. In other words time scale became relatively small where TKE was large.

Figure 7 shows the modeled time scale, TKE, and concentration distributions for a building of 30 m cube. Concentration distributions were obtained with the modeled and a constant time scale. As seen from Fig. 7, concentration distributions are similar if appropriate constant value was selected. An optimum value was selected by performing several trial simulations.

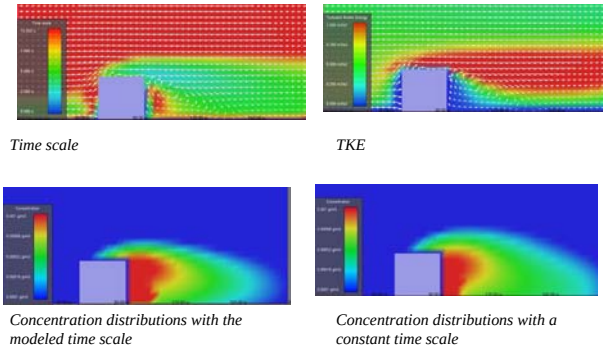

Fig. 7: The modeled time scale, TKE, and concentration distributions. Concentration distributions were obtained with the modeled time scale (left) and a constant time scale (right). The dimension of the building was a 30 m cube.

The modeled time scale represented the time scale in the vertical direction. The same numerical values were used for the horizontal directions, because the horizontal and vertical grid spacing was identical (4 m). It was anticipated that horizontal time scale could be obtained by multiplying the grid spacing ratio to the modeled time scale. This assumption need to be tested in the future.

4. SUMMARY

A2Cflow was improved by including not only the production terms in the vertical but also in the horizontal directions in the turbulence kinetic energy and length scale equations.

Airflows around rectangular blocks of different dimensions in a wind tunnel were simulated with horizontal grid spacing of 1 cm. Reattachment distance behind blocks was in good agreement with those predictedby the standard k-e model, but was larger in comparison with wind tunnel data.

The Lagrangian integral time was determined as the ratio of the length scale to the square root of TKE. This approach removed ambiguity associated in selecting an optimum constant value by trial and error to match the computed with the observed concentration distributions.

The Lagrangian integral time in the horizontal directions were proposed to be proportional to the time scale in the vertical direction multiplied by the grid spacing ratio. This assumption remained to be tested in the future.

REFERENCES

Architectural Institute of Japan, 2007: Guidebook for Practical Applications of CFD to Pedestrian Wind Environment around Buildings, 207pp (in Japanese).

Hirt, C.W., and J. L. Cox, 1972: Calculating Three-Dimensional Flows around Structures and over Rough Terrain. *J. of Computational Phys*., **10**, 324-340.

Kao, C.-Y. J. and Yamada, T., 1988: Use of the CAPTEX Data for Evaluation of a Long-Range Transport Numerical Model with a Four-Dimensional Data Assimilation Technique, *Monthly Weather Review*, **116**, pp. 293-206.

Mellor, G. L., and T. Yamada, 1974: A Hierarchy of Turbulence Closure Models for Planetary Boundary Layers. *J. of Atmos. Sci*., **31**, 1791-1806.

Mellor, G. L., and T. Yamada, 1982: Development of a Turbulence Closure Model for Geophysical Fluid Problems. *Rev. Geophys. Space Phys*., **20**, 851-875.

Murakami, S., 2000: Computational Environment Design for Indoor and Outdoor Climates. The University of Tokyo Press, 443pp (in Japanese).

Tominaga, Y., A. Mochida, R. Yoshie, H. Kataoka, T. Nozu, M. Yoshikawa, and T. Shirasawa, 2008: AJI guidelines for practical applications of CFD to pedestrian wind environment around buildings. J. Wind Eng. and Industrial Aerodynamics, 96, 1749-1761.

Yamada, T., 1983: Simulations of Nocturnal Drainage Flows by a q^2l Turbulence Closure Model. *J. of Atmos. Sci*., **40**, 91-106.

Yamada, T., 2004: Merging CFD and Atmospheric Modeling Capabilities to Simulate Airflows and Dispersion in Urban Areas. *Computational Fluid Dynamics Journal,* **13 (2):47**, 329-341.

Yamada, T., 2008: Numerical simulations of airflows and transport of airborne materials in the exterior and interior of buildings in complex terrain, American Met. Soc. Annual meeting, New Orleans.

Yamada, T., and S. Bunker, 1988: Development of a Nested Grid, Second Moment Turbulence Closure Model and Application to the 1982 ASCOT Brush Creek Data Simulation. *Journal of Applied Meteorology*, **27**, 562-578.